Strontium-loaded magnesium phosphate bone cements and effect of polymeric additives

Strontium-loaded magnesium phosphate bone cements and effect of polymeric additives

Rita Gelli, Giulio Bernardini, Francesca Ridi*

Department of Chemistry "Ugo Schiff" and CSGI, University of Florence
Via della Lastruccia 3, 50019, Sesto Fiorentino, Florence, Italy

***Corresponding author**
Francesca Ridi
E-mail: francesca.ridi@unifi.it
Tel: +39 055 4573015
Address: Department of Chemistry "Ugo Schiff" and CSGI, University of Florence, via della Lastruccia 3, Sesto Fiorentino, 50019 Florence, Italy.

Abstract

Magnesium phosphate-based cements (MPCs) are nowadays regarded as promising materials in the field of bone repair. The inclusion of Sr ions in the formulations may represent a valuable strategy to improve their bone regeneration performances, but the effect that such ion exerts on the physico-chemical properties of the material have not been investigated so far. In this work we describe the development of Sr-MPCs obtained including Sr ions in different forms, i.e., using Sr-substituted tri-magnesium phosphate precursor powder or including in the formulation Sr-based salts ($SrCl_2$ and $SrHPO_4$). The materials were characterized both in the form of pastes and hardened cements, finding that according to the type of Sr precursor used we can tune the setting time, the amount of binding phases in the cements, their morphology and thermal behavior. The dissolution behavior and the release kinetics of Mg^{2+} and Sr^{2+} can as well be modulated, and in particular the use of $SrCl_2$ in the formulation leads to a higher dissolution and a faster release of a significant amount of both Mg^{2+} and Sr^{2+}, compared to the other samples. Given the unsatisfying performances obtained during the injectability and anti-washout tests, we also included two polymeric additives, namely poly(N-isopropylacrylamide) and mucin, in the Sr-MPCs formulations. The results demonstrate that it is possible to obtain Sr-MPCs with promising properties for applications as bone cements, that can be tuned according to the form under which Sr is included in the formulation. In addition, mucin markedly improves the cohesion

Abbreviations: CaPs: Calcium Phosphates; MgPs: Magnesium Phosphates; MPCs: Magnesium Phosphate Cements; CPCs: Calcium Phosphate Cements; PNIPAm: Poly(N-isopropylacrylamide); TMP: Trimagnesium Phosphate; RT: Room Temperature; P/L: Powder to liquid; XRD: X-Ray Diffraction; PDF: Powder Diffraction Files; FT-IR: Fourier Transform - Infrared Spectroscopy; SD: Standard Deviation; FE-SEM: Field Emission - Scanning Electron Microscopy; TGA: Thermogravimetry; DSC: Differential Scanning Calorimetry; PBS: Phosphate-Buffered Saline; ICP-AES: Inductively Coupled Plasma – Atomic Emission Spectroscopy.

and injectability of the Sr-MPC pastes, providing a simple but effective strategy to develop materials of interest in the orthopedic field.

Keywords
Magnesium Phosphates; Bone cements; Strontium; Polymers.

1. Introduction

The repair of bone tissue is a complex phenomenon in which different types of biomaterials can be used depending on the specific need. Together with long-term stable grafts made of metals, alloys or ceramics, biodegradable materials which can be resorbed and replaced over time by the body's own regenerated tissue also play a fundamental role. Calcium Phosphate (CaP)-based materials have been widely used to this purpose, thanks to their chemical similarity with bone inorganic matrix that consists of poorly-crystalline hydroxyapatite [1]. Despite the significant advantages associated to CaPs, it was often reported that their low solubility may cause a slow degradation of the biomaterial, eventually hampering bone regeneration processes [2]. To overcome this drawback, Magnesium Phosphates (MgPs) have been recently suggested as a promising alternative to CaP for bone repair [3–5]. Mg^{2+} is the fourth most abundant ion in the human body and it is mainly located in bone (53%), muscles (27%) and soft tissues (19%) [6]. MgPs share some similarities with CaPs but they are endowed with a higher solubility that makes them attractive for the preparation of biodegradable bone repair materials, including ceramics, scaffolds, cements and coatings [3]. Among them, Magnesium Phosphate Cements (MPCs) can be used to fill bone voids or stabilize fractures and represent an interesting alternative to the well-established Calcium Phosphate Cements (CPCs). MPCs can be easily prepared by mixing a powder (MgO or $Mg_3(PO_4)_2$) and a liquid component, typically an aqueous solution of a phosphate salt [2]. The reaction between them leads to the formation of a paste that in time sets, forming a hard and compact material. Bone cements should be biocompatible, biodegradable, bioactive, osteoconductive, able to set in physiological conditions, injectable and moldable. Even if the research concerning MPCs application in the biomedical field is in the early stages, these materials have already demonstrated to fulfill many of such properties. Moreover, magnesium plays a pivotal role in bone calcification and in increasing bone density, CaP formation, and in bone cell adhesion and stability [2,7]. Mg^{2+} is not the sole ion that has an effect in bone formation processes [8]. Sr^{2+} is also relevant to bone metabolism, as it reduces the differentiation and activity of osteoclasts and it enhances the metabolic activity of osteoblasts [9–11]. It is administrated as a treatment for osteoporosis under the form of strontium ranelate, which stimulates bone formation, improves bone microarchitecture by increasing the quality of bone tissue, hampers bone loss and reduces the differentiation and resorption activity of osteoclasts [12]. The oral administration of such drug is though associated to an increased risk of adverse cardiovascular events, making it necessary to develop strategies to achieve a local release.

In the literature, several Sr-substituted CPCs have already been described [13–22], while the inclusion of such ion in MPCs was investigated to a much lesser extent. Some reports describe the preparation of bioceramics based on $Mg_xSr_{3-x}(PO_4)_2$ powders which show promising performances towards bone regeneration both *in vitro* and *in vivo* [23–25]. Coatings made of Sr-doped struvite ($MgNH_4PO_4 \cdot 6H_2O$) applied on titanium surfaces to improve bone integration were also reported [26,27], as well as scaffolds based on $Mg_3(PO_4)_2/Mg_2Sr(PO_4)_2$ microspheres [28] and Sr doped Mg-MgP composites [29]. Such examples testify the importance of Sr inclusion in biomaterials but refer to systems markedly different from bone cements. Concerning specifically MPCs, particularly relevant are the works by Meininger *et al.* which describe Sr-substituted magnesium phosphate scaffolds prepared by 3D powder printing using $Mg_xSr_{3-x}(PO_4)_2$ as a starting material [7,30]. In such works, the properties of the final scaffolds obtained from the hardening of the powder in the binder solution are characterized, resulting in an improved clinical applicability and biological performances. Nevertheless, to the best of our knowledge, the effect of Sr on the features of MPCs pastes was never addressed so far. This aspect is though crucial to tailor the properties of the materials in view of the clinical application where, for example, the possibility of molding and injecting bone cements is regarded as one of their main advantages, allowing for their use in minimally invasive surgery. The formulation of phosphate-based injectable bone cements is not straightforward, as they often show a limited extrusion capacity and encounter phase separation issues [31–33]. This phenomenon occurs during injection when the extruded paste is more liquid-like than the one loaded in the syringe, resulting in the formation of a dense cake of particles at the plunger side and eventually leading to non-homogeneity of the extrudate, variation from the initial powder to liquid ratio, modifications in the cement setting and properties, and halting of the injection because of syringe plugging [34]. Strategies to limit such phenomenon include decreasing the powder to liquid ratio, the particles size and the injection rate, increasing the viscosity of the liquid or the repulsive force between the particles, improving barrel geometry, and agitating the paste throughout extrusion [32]. When choosing a method to improve injectability, it is important to consider how it would impact the other cement properties and if it would be doable in a surgical application. The inclusion of polymeric additives in the cement formulations is one of the most exploited strategies for improving CPCs injectability and cohesion [35–40], whereas for MPCs, this aspect was investigated to a limited extent [41]. Ideally, polymers included in bone cements to improve the extrusion process should also be biocompatible and not hamper the other cement properties.

The aim of this work is to develop Sr-containing MPCs and polymeric additives, to obtain injectable cements to be applied in the orthopedic field. Sr was included in MPCs with different strategies, *i.e.,* using $Mg_{2.5}Sr_{0.5}(PO_4)_2$ and $Mg_2Sr(PO_4)_2$ as starting powders and including Sr salts ($SrCl_2$ and $SrHPO_4$) in $Mg_3(PO_4)_2$-based formulations. Such systems were studied in terms of setting time, cohesion, crystallinity, thermal properties, and morphology. The kinetics of Mg^{2+} and Sr^{2+} released from the cements upon incubation in an aqueous medium were also investigated, as well as their resistance to dissolution. Since the injectability and anti-washout performances of the developed Sr-MPCs was not satisfying, we also studied the possibility of including polymeric additives in the formulation, namely poly(N-isopropylacrylamide) (PNIPAm) and mucin. PNIPAm was selected because of its biocompatibility and thermoresponsive nature, as it shows a lower critical

solution temperature of 32 °C, meaning that it undergoes a sol-gel transition close to physiological temperature [42]. The idea was to understand if the presence of PNIPAm in MPCs extruded at 37 °C would provide integrity and resistance to dissolution to the cement paste due to polymer gelification. Mucin, the biopolymer that is the main component of the mucus hydrogel-like layer that coats the wet epithelial surfaces of our body [43], was chosen because of its lubrication properties which could, in principle, facilitate the extrusion process. Sr-MPCs containing both polymers were tested for their injectability, cohesion and anti-washout properties. Our results show how the use or different Sr precursors impacts the most important properties of MPCs and showcase the use of polymeric additives to improve the performances of MPCs.

2. Materials and methods

2.1 Materials

Newberyite ($MgHPO_4 \cdot 3H_2O$, purity ≥ 97%), $SrCO_3$, (purity ≥ 98%), $(NH_4)_2HPO_4$ (DAHP, purity ≥ 98%) NaCl (purity ≥ 99.5%), KCl (purity ≥ 99%), $Na_2HPO_4 \cdot 12H_2O$ (purity ≥ 99%) and $KH_2PO_4 \cdot H_2O$ (purity ≥ 99%) were purchased from Sigma Aldrich. $Mg(OH)_2$ (purity ≥ 95%) and $CaCl_2$ (purity ≥ 97%) were obtained from Fluka while $SrCl_2 \cdot 6H_2O$ (purity > 99%) was supplied by Riedel-de Haën. $NaHCO_3$ (purity ≥ 99.5%) was obtained from Merck. Mucin from porcine stomach (Type II) and Poly(N-isopropylacrylamide) (PNIPAm, average Mn 7,000) were also purchased from Sigma-Aldrich.

2.2 Powders calcination

TMP (Tri-magnesium phosphate, $Mg_3(PO_4)_2$) and Sr-TMP were prepared by means of calcination starting from $MgHPO_4 \cdot 3H_2O$, $SrCO_3$ and $Mg(OH)_2$. The powders were mixed according to the amounts given in Table 1, adapting the procedure by Meininger *et al.* for the Sr-containing samples [7]. The powders were thoroughly mixed and placed in ceramic crucibles for calcination at 1050 °C for 5 h. After quenching at room temperature (RT), the sintered cakes were grinded with agate mortar and pestle and sieved with a 150 µm sieve.

Table 1. Composition of the calcinated powders.

Sample	Composition $Mg_{(3-x)}Sr_x(PO_4)_2$	$MgHPO_4 \cdot 3H_2O$ (g)	$Mg(OH)_2$ (g)	$SrCO_3$ (g)	$MgHPO_4 \cdot 3H_2O$ (mol)	$Mg(OH)_2$ (mol)	$SrCO_3$ (mol)
TMP_0	$Mg_3(PO_4)_2$ (x=0)	10.46	1.74	-	0.06	0.030	-
TMP_0.5	$Mg_{2.5}Sr_{0.5}(PO_4)_2$ (x=0.5)	10.46	0.875	2.214	0.06	0.015	0.015
TMP_1	$Mg_2Sr(PO_4)_2$ (x=1)	10.46	-	4.429	0.06	-	0.030

2.3 Preparation of $SrHPO_4$ crystals

$SrHPO_4$ crystals were obtained by dissolving 1.6 g of $SrCl_2 \cdot 6H_2O$ in 3 mL of 3.5 M DAHP solution. Upon dissolution of the salt, the solution immediately gets turbid. The dispersion was kept under stirring for few

minutes and the solid precipitate was collected by filtration, washing, centrifugation and drying. XRD and FE-SEM results reported in Figure S1 confirmed the nature of the obtained product.

2.4 Preparation of Sr-MPCs

Five types of MPCs including Sr under different forms were prepared. Three samples were obtained using calcinated powders (TMP_0, TMP_0.5 and TMP_1, see section 2.2), by mixing 0.5 g of powder with 0.333 mL of DAHP 3.5 M at powder to liquid (P/L) ratio of 1.5 g/mL (see Table 2). Sr-MPCs obtained by inclusion of Sr-salts were prepared by carefully mixing TMP_0 with either $SrCl_2$ or $SrHPO_4$ by homogenizing them with mortar and pestle for 2 min (amounts reported in Table 2). Different amounts of the two salts were used to obtain final samples with the same Mg/Sr atomic ratio. In these samples, the amount of DAHP 3.5 M was increased to keep P/L ratio at 1.5 g/mL, considering that the powder accounts for both TMP and the Sr-salt. The pastes were transferred into plastic molds (diameter 1.2 cm, height 0.7 cm) and let set at 37 °C and relative humidity > 96% for at least 3 days before characterization.

Table 2. Composition of the samples under investigation in this work.

	TMP_0 (g)	**TMP_0.5 (g)**	**TMP_1 (g)**	**$SrCl_2 \cdot 6H_2O$ (g)**	**$SrHPO_4$ (g)**	**DAHP 3.5 M (mL)**	**Mg/Sr**
MPC_0	0.5	-	-	-	-	0.333	-
MPC_0.5	-	0.5	-	-	-	0.333	5
MPC_1	-	-	0.5	-	-	0.333	2
MPC_$SrCl_2$	0.5	-	-	0.177	-	0.451	8.6
MPC_$SrHPO_4$	0.5	-	-	-	0.123	0.415	8.6

For the preparation of Sr-MPC with mucin and PNIPAm, the same procedure was used, except for the fact that the polymers were mixed with the powder component and homogenized with mortar and pestle for two minutes. The final concentration of the polymers was 10% w/v (v=DAHP 3.5 M volume).

2.5 Characterization techniques

2.5.1 X-Ray Diffraction (XRD)

XRD patterns were collected using a D8 Advance with DAVINCI design (Bruker), with an X-ray source at λ=1.54 Å (Cu Kα radiation). The X-ray source operated at 40 kV and 40 mA. The diffractograms were collected in the 2θ range 5° - 60°, with a step size of 0.03° and a time/step of 0.3 s. Samples were grinded using agate mortar and pestle and flattened on a Si low background sample holder. The phases were assigned with Powder Diffraction Files (PDF) from the International Centre for Diffraction Data.

2.5.2 Attenuated Total Reflection -Fourier Transform Infrared Spectroscopy (ATR-FTIR)

ATR-FTIR spectra were collected with a Nexus Thermo-Nicolet 870 FT-IR spectrophotometer equipped with a MCT detector cooled with liquid N_2 and a Golden Gate. The spectra were collected in the 4000-650 cm^{-1} range, with 128 scans and a spectral resolution 2 cm^{-1}.

2.5.3 Laser granulometry

The size distribution of the calcinated powders was analyzed by means of laser granulometry, using a Mastersizer 3000 (Malvern) with a Hydro SM dispersion unit. Propan-2-ol (refractive index at 20 °C: 1.375) was used as dispersant. Measurements were conducted using a stirring speed of 1800 rpm, and for each sample 20 runs of 10 s each were averaged. Before adding the sample, the background (propan-2-ol) was measured for 15 s, then the sample was added until an obscuration of ~4% was attained. The results are expressed as D_{10}, D_{50} and D_{90} (average ± standard deviation (SD) of the 20 measurements).

2.5.4 Field Emission-Scanning Electron Microscopy (FE-SEM)

FE-SEM was carried out using a Zeiss ΣIGMA FE-SEM (Carl Zeiss Microscopy GmbH), with an accelerating voltage of 2.0 kV, a sample-detector distance ~ 2 mm and using the in-Lens detector. Cross-sections of the cements were fixed on aluminum stubs by means of conductive tape.

2.5.5 Setting time

The initial (t_1) and final (t_2) setting time of the cements were obtained by means of a Gillmore apparatus (Matest), following the ASTM standard C-266. Immediately after preparation, cement pastes were transferred in plastic molds (diameter 1.1 cm) and set at T=37 °C and relative humidity > 96%. Every minute, samples were removed from the incubation chamber and tested with the Gillmore apparatus. The cement is considered to have attained its initial or final setting time when its surface respectively bears the initial or final Gillmore needle without appreciable indentation (initial needle Ø=2.12 mm, weight 113 g and final needle Ø=1.06 mm, weight 453.6 g).

2.5.6 Thermal analysis

Thermal analysis was carried out by means of Simultaneous Thermogravimetry/Differential Scanning Calorimetry (TGA/DSC) with a SDT Q600 from TA Instruments. Grinded samples were placed in alumina pans and analyzed from RT to 1000 °C, with a ramp of 10 °C/min, in N_2 atmosphere (flow rate 100 mL/min).

2.5.7 Extrusion

The spreading degree of the pastes after extrusion was evaluated by injecting them with a syringe onto graph paper and measuring the diameter of the extruded cylinder using ImageJ. The procedure of paste preparation and syringe loading was analogous to the injectability tests described in section 2.5.8. The difference between the diameter of the extruded cylinder and the syringe opening (2 mm) was taken as an indication of the degree of paste spreading upon extrusion.

2.5.8 Injectability

For the injectability test, the pastes were prepared by mixing the powder and the liquid components for 30 s according to the composition reported in Table 2. The obtained cement was quickly transferred into the barrel of a plastic syringe with a 3 mL volume and aperture of 2 mm. No needle was used for the test, as for clinical applications bone cements are commonly injected through cannulated needles which have an internal diameter of 1.80 – 3.43 [32]; therefore, the aperture of the syringe was sufficient to mimic the injection process. The paste was extruded by application of a manual load after 5 min from the beginning of the mixing procedure. The injectability of the pastes was quantified according to equation 1[44].

$$I(\%) = \frac{m_{injected}}{m_{initial}} \times 100$$ Equation 1

The syringe was weighed *i.* before loading it with the paste (m_1); *ii.* after loading it with the paste (m_2); *iii.* after extrusion (m_3). The $m_{injected}$ was obtained as m_2-m_3 while $m_{initial}$ was m_2-m_1. The dead volume of the syringe was estimated performing some preliminary tests, which showed that pastes can be considered as completely injectable when I(%) is 85%.

2.5.9 Anti-washout test

The anti-washout tests were carried out by manually extruding the cement pastes with a syringe in Ringer solution, which was prepared by dissolving NaCl (6.8 g/L), KCl (0.4 g/L), $CaCl_2$ (0.2 g/L) and $NaHCO_3$ (1 g/L) in MilliQ water. The pH, estimated with litmus paper, was ~7.3. Cement pastes were prepared and loaded in a syringe as already described for the injectability test (see section 2.5.8). After 5 min from the mixing, the pastes were extruded in a Petri dish containing 10 mL of Ringer solution. The test was carried out by extruding the paste in the Ringer solution at both RT and 37 °C. The appearance of the extruded paste was assessed after 30 min of immersion in the Ringer solution.

2.6 Dissolution and release experiments

Sr-MPCs were incubated in PBS (Phosphate-Buffered Saline) at 37 °C to determine the extent of the dissolution and to study the release kinetics of Mg^{2+} and Sr^{2+}. 250 mL of PBS (1x) were prepared following the standard recipe and dissolving NaCl (137 mM), KCl (2.7 mM), $Na_2HPO_4 \cdot 12H_2O$ (10 mM) and $KH_2PO_4 \cdot H_2O$ (1.8 mM) in Milli-Q water. MPCs specimens were prepared following the procedure reported in section 2.4, but since smaller molds were used (diameter 0.8 cm, height 0.7 cm), the amounts of reactants reported in Table 2 were halved. After 5 days of setting, cements were de-molded, weighted and immersed in 20 mL of PBS inside a glass vial. The experiment was carried out at 37 °C and 5 mL of PBS were collected from each sample after 7 h, 1 day, 4 days, 7 days, 14 days, 28 days, and 56 days. Each aliquot was replaced with 5 mL of fresh PBS to keep constant the total volume (20 mL). At the end of the test, MPCs were dried at RT until a constant weight was reached, and the weight loss was calculated by comparing their weight before and after incubation. Each sample was prepared in triplicate, and the obtained results were averaged.

The determination of released Mg^{2+} and Sr^{2+} was carried out by analyzing in triplicate the collected aliquots by Inductively Coupled Plasma – Atomic Emission Spectroscopy (ICP-AES) using a Varian 720-ES. An amount of 250 µL of samples was diluted to 5 mL with 0.1% suprapure nitric acid obtained by sub-boiling distillation, spiked with 1.0 ppm of Ge used as an internal standard, and analyzed. Calibration standards were prepared by gravimetric serial dilution from commercial stock standard solutions of Sr and Mg at 1000 mg/L. The wavelengths used for elements determination were 407.771 nm for Sr, 279.553 nm for Mg, and 209.426 nm for Ge. The operating conditions were optimized to obtain maximum signal intensity, and between each sample, a rinse solution constituted by 2% v/v HNO_3 was used.

The data were plotted as cumulative concentration (mg/mL) of released Mg/Sr or cumulative % vs time, where the % was calculated by dividing the amount of Mg/Sr determined at time t by the amount of Mg/Sr present in the cements before incubating them in PBS. The cumulative concentration was calculated by adding to the amount of Mg/Sr found at time t the amount of Mg/Sr removed in the previous withdrawal.

3. Results and discussion

3.1 Characterization of the calcinated powders

The Sr-containing TMP was obtained by means of a calcination reaction, readapting the protocol from the work of Meininger *et al.* [7] (see section 2.2). The powders were characterized in terms of crystallinity, size and morphology, and the results are reported in Figure 1. The XRD pattern of TMP_0 (Figure 1A) shows the peaks typical of $Mg_3(PO_4)_2$ (Farringtonite, PDF 04-010-3790), whereas the diffractogram of sample TMP_0.5 also displays signals corresponding to $Mg_2Sr(PO_4)_2$. The pattern of TMP_1 is more complex than the previous ones, showing a variety of peaks compatible with $Mg_2Sr(PO_4)_2$, $Mg_3Sr_{18}(PO_4)_{14}$, $Sr_2P_2O_7$, and $Mg_2Sr(PO_4)_2$. This sample thus consists of mixed strontium and magnesium phosphate phases, even if it is difficult to precisely identify their exact nature due to the large number of signals and their overlap present in the pattern.

FTIR spectra are given in Figure 1B: TMP_0 shows a broad signal between 880 cm^{-1} and 1200 cm^{-1} compatible with PO_4^{3-} stretching, in agreement with $Mg_3(PO_4)_2$ spectrum reported in the literature [45]. The spectra of samples TMP_0.5 and TMP_1 show additional signals at 1440 cm^{-1} and 855 cm^{-1}, which are consistent with carbonate vibrations [46]. The presence of CO_3^{2-} could be due to the carbonation of the calcined product upon storage, and was likely not observed in the XRD patterns because of the superimposition of $SrCO_3$ peaks with signals coming from $Mg_3(PO_4)_2$ and $Mg_2Sr(PO_4)_2$ [47]. The possibility that some residual $SrCO_3$ is present in the calcined powders can be reasonably ruled out, as its decomposition to SrO and CO_2 starts at about 730 °C [48,49].

The size and the morphology of the calcinated powders were determined by means of laser granulometry and FE-SEM, respectively. The results from granulometry shown in Figure 1C reveal that the three samples have a broad size distribution with the maxima centered at about 90 µm for TMP_0.5 and TMP_1 and 70 µm for TMP_0. The D_{10}, D_{50} and D_{90} values are reported in Table S1 in the Supplementary Material. FE-SEM micrographs in Figure 1D, 1E and 1F show that the powders are characterized by an irregular morphology, with both large smooth crystals and small rough structures. The irregular shapes are not surprising considering their preparation procedure which involves calcination, grinding and sieving (see section 2.2).

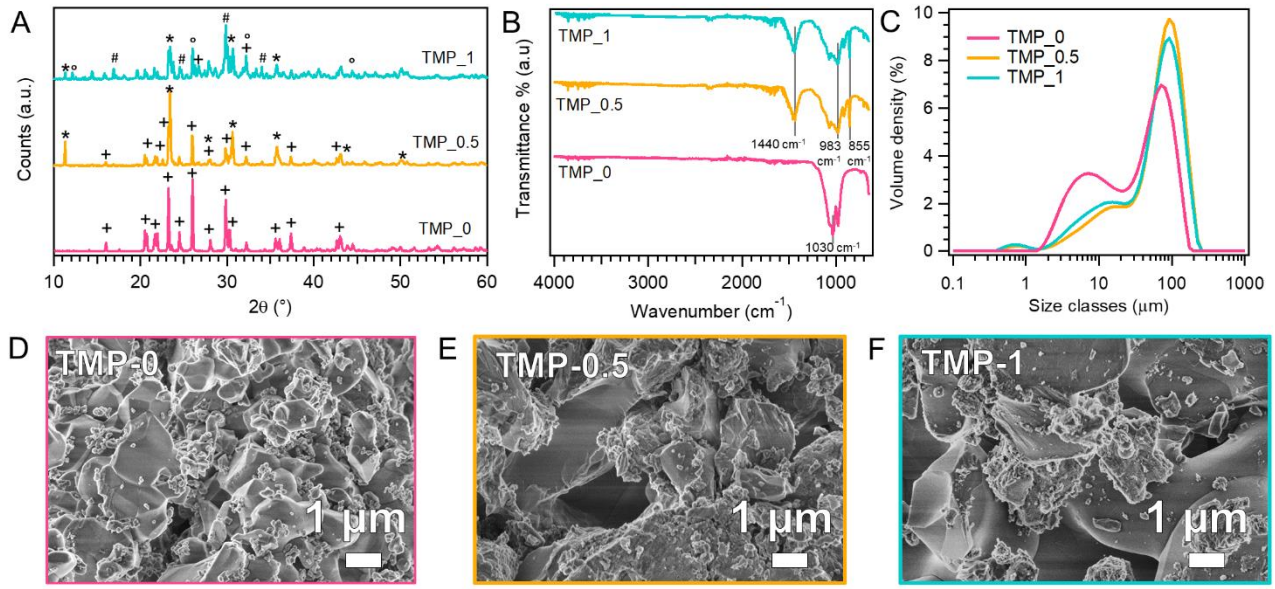

Figure 1. Characterization of the calcinated powders. A) XRD patterns of (from the bottom to the top) TMP_0, TMP_0.5, TMP_1. The patterns have been vertically offset for display purposes. The legend of the symbols is the following: + $Mg_3(PO_4)_2$ PDF 04-010-3790, * $Mg_2Sr(PO_4)_2$ PDF 00-014-0206, ° $Sr_2P_2O_7$ PDF 04-013-3761, # $Mg_3Sr_{18}(PO_4)_{14}$ PDF 00-058-0834. B) ATR-FTIR spectra of (from the bottom to the top) TMP_0, TMP_0.5, TMP_1. The curves have been vertically offset for display purposes. C) Size distribution curves of the calcinated samples obtained by laser granulometry. D, E, F) FE-SEM micrographs of TMP_0, TMP_0.5, TMP_1.

3.2 Characterization of Sr-MPCs

As described in section 2.4, Sr-MPCs were prepared either using Sr-containing calcinated precursor powders or including Sr-based salts in the classical TMP-based recipe. The appearance and spreading of the pastes were evaluated by transferring them immediately after mixing on graph paper. The photos reported in Figure 2A show that MPC_0 (*i.e.*, reference sample without Sr), MPC_0.5 and MPC_$SrHPO_4$ have a similar cohesion degree, while MPC_$SrCl_2$ is more compact and has a toothpaste-like consistency. MPC_1, on the other hand, is more solid-like and does not spread uniformly. The pastes, in time, set and harden forming a solid cement. The setting times were measured by means of the Gillmore method, and the results reported in Figure 2A and Table S2 show that Sr-MPCs obtained by Sr-salt inclusion have an initial and final setting time similar to the reference sample MPC_0 and, out of note, in line with clinical needs for bone cements [50]. In fact, in these samples the inclusion of Sr only results in a slight increase of the final setting time. In contrast, MPCs prepared with Sr-containing calcinated powders (*i.e.*, MPC_0.5 and MPC_1) have a markedly delayed setting and, for MPC_1, it was not possible to observe setting within 1 h. In MPCs, the setting and hardening are caused by the formation and entanglement of crystalline phases formed upon the reaction of the precursor powder and the liquid component. It is known from the literature that the reaction between TMP and DAHP leads to the formation of struvite ($MgNH_4PO_4 \cdot 6H_2O$) as cement binding phase [2,44,51,52]. By means of XRD and FTIR we investigated the phases formed in Sr-containing MPCs. The XRD patterns shown in Figure 2B reveal that,

as expected, all the peaks of MPC_0 are ascribable to struvite and TMP (see the comparison of the patterns in Figure S3A). Interestingly, all Sr-MPC samples display struvite characteristic peaks (see Figure S2), together with those of the unreacted precursor powders. In MPC_$SrCl_2$ the signals due to the Sr salt cannot be detected [53], whereas MPC_$SrHPO_4$ also displays small peaks characteristic of $SrHPO_4$ (see Figure S2E). We can thus conclude from XRD analyses that despite the presence of Sr, the binding phase that forms in cements still consists of struvite crystals, as no new binding phase containing Sr can be detected. FTIR spectra given in Figure S3 confirm such findings, as the peaks typical of struvite are present in all samples, namely a broad band between 3550 and 2400 cm^{-1} due to O-H and N-H stretching, a peak at 1430 cm^{-1} related to N-H bending, an intense signal centered at 984 cm^{-1} due to PO_4^{3-} stretching, and a broad peak between 800 and 650 cm^{-1} compatible with water libration modes [54]. The only meaningful difference between samples' spectra can be found in the shape of the peak around 1000 cm^{-1} for sample MPC_1, which is broader and displays several shoulders, in agreement with XRD that showed weak struvite signals in such sample.

An indication of the amount of formed struvite in the samples can be obtained by means of thermogravimetry (see Figure 2C). For the samples prepared from the calcinated powders we can assume that the weight loss occurring in the cement samples upon heating is entirely ascribed to the products formed during cement setting, as the precursor powders are not expected to lose weight since they were prepared at high temperatures and already experienced a T=1000 °C. The thermogram of the reference sample (MPC_0, red curve in Figure 2C) shows that the weight loss mainly occurs between 60 °C and 150 °C, and can be ascribed to the loss of H_2O and NH_3 molecules from struvite [55]. At 1000 °C, the weight loss is 31% (see Figure 2D and Table S2). Considering that a complete loss of the volatile components from pure struvite sample would result in a weight loss of 51% [55], we can estimate that MPC_0 contains 61% of struvite. For MPC_0.5 and MPC_1 we obtain a struvite amount of 60% and 34%, respectively. Such results are in line with the enthalpy of the exothermic peak observed for all samples in the heat flow profiles at ~ 670 °C, that is due to the crystallization of amorphous $MgHPO_4$ formed upon struvite decomposition (see the dashed lines in Figure 2C and the calculated enthalpies in Figure 2D and Table S2). The area of such peak, that is strictly connected to struvite amount in the samples, is similar for MPC_0 and MPC_0.5, while it is lower for MPC_1, in agreement with a limited formation of struvite in such sample. For MPC_$SrCl_2$ and MPC_$SrHPO_4$ the situation is different, since part of the observed weight loss might be due to the thermal degradation of the two salts, and not only to struvite (see the thermograms of $SrCl_2$ and $SrHPO_4$ in Figure S4). Therefore, in these cases the estimation of struvite amount in the cements from the weight loss is not straightforward. The observation of the enthalpy values, though, suggests a smaller conversion degree to struvite with respect to sample MPC_0, indicating that the presence of Sr salts somehow limits the extent of TMP and DAHP reaction.

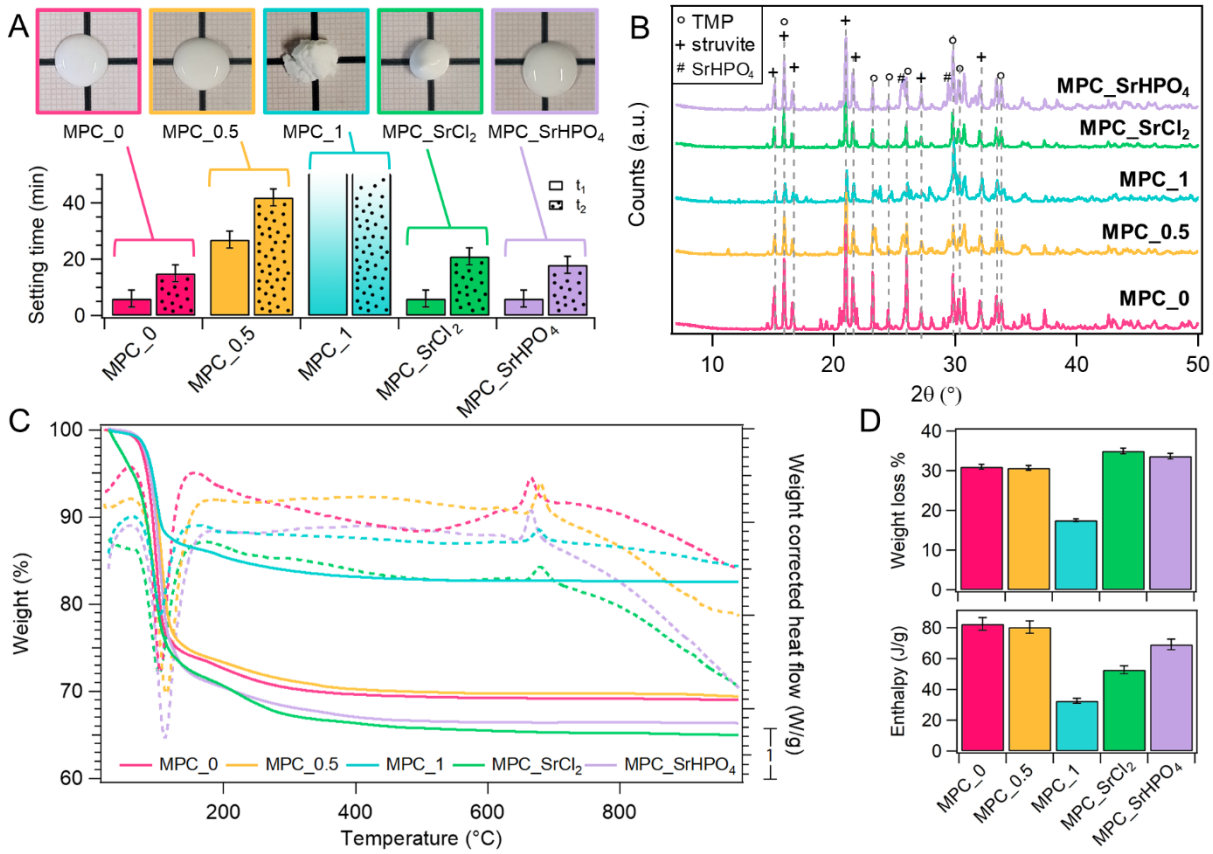

Figure 2. A) On the top, the appearance of the cement pastes immediately after preparation. The size of each photo is 2 cm x 2 cm. Below, the initial (solid) and final (dotted) setting times of the cements as obtained by the Gillmore test. B) XRD patterns of (from the bottom to the top) MPC_0, MPC_0.5, MPC_1, MPC_$SrCl_2$, MPC_$SrHPO_4$ (see the color legend at the bottom of the figure). The diffractograms have been vertically offset for display purposes. The reference patterns of TMP (°), struvite (+) and $SrHPO_4$ (#) are given in Figure S2. C) TGA (solid curves, left y axis) and DSC (dashed lines, right y axis, exo up) curves of the Sr-MPC samples. D) Thermal analysis results: weight loss % between RT and 1000 °C (top) and enthalpy associated with the exothermic peak at about 670 °C in the DSC curve (bottom). The associated error bars are related to the instrumental error (2 % of the value for the weight loss and 5 % of the value for the enthalpy).

The morphology of cements cross-sections was observed on the micrometric scale by means of FE-SEM (see Figure 3). MPC_0 (Figure 3A) shows objects of several microns endowed with inner cracks and porosities, that are typical of struvite crystals [56]. Similar features are observed in all samples, in agreement with XRD and FTIR findings. MPCs containing Sr have a more heterogenous morphology, and different type of objects are observed: in MPC_0.5, fan-shaped structures (see the arrows in Figure 3B and a high magnification micrograph in Figure S5A) accompany struvite crystals. Since these peculiar structures were not observed in the precursor powder TMP_0.5 (see Figure 1E), their formation reasonably occurs during the cement setting reaction. Sample MPC_1 (Figure 3C) displays rounded objects together with small amounts of struvite crystals, that might be related to Sr-containing phases formed during setting or to unreacted TMP_1 (see Figure S5B). The morphology of sample MPC_$SrCl_2$ (Figure 3D and 3E) is very peculiar. In addition to struvite crystals, it

is possible to observe a layer that covers smaller and irregular structures: we hypothesize that in this sample struvite begins to crystallize around $SrCl_2$ grains, forming a sort of layer that partially covers them. Finally, in sample MPC_$SrHPO_4$ (Figure 3F) it is possible to observe rod-like crystals that are compatible with $SrHPO_4$ morphology (see Figure S1C and Figure S5C).

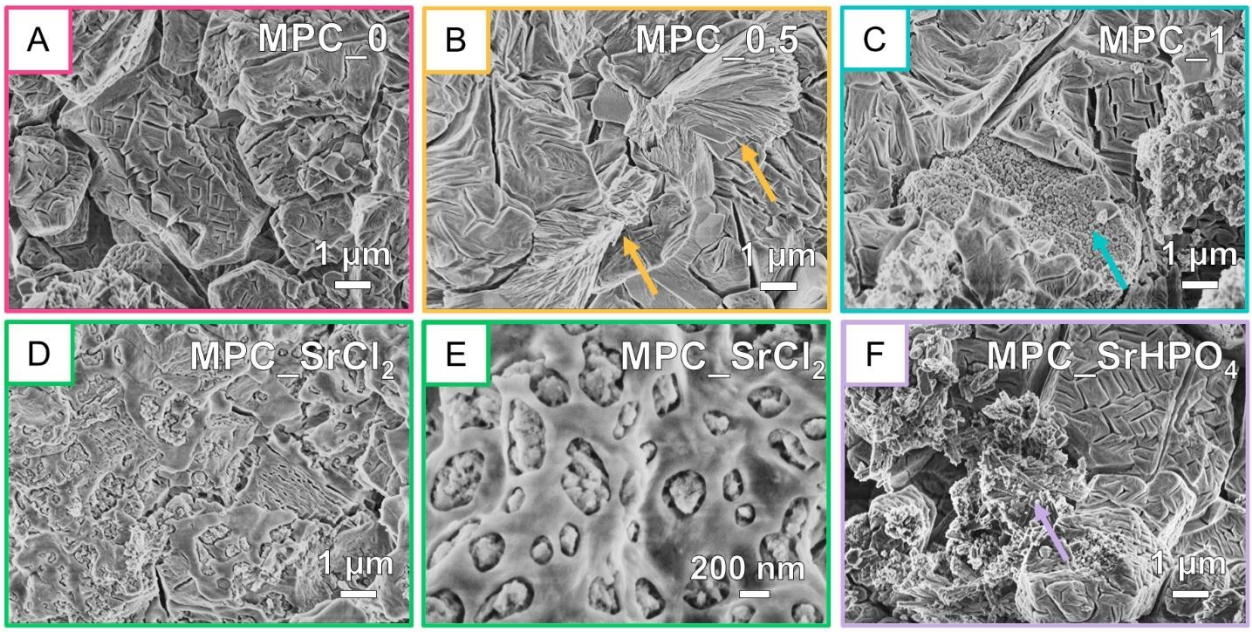

Figure 3. FE-SEM micrographs of A) MPC_0, B) MPC_0.5, C) MPC_1, D) MPC_$SrCl_2$, E) MPC_$SrCl_2$ – high magnification F) MPC_$SrHPO_4$. The regions highlighted by the arrows are visible at higher magnification in Figure S5.

3.3 Dissolution and release experiments

When bone cements are used in clinics, they will get in contact with biological fluids, and they will begin a slow dissolution process accompanied by the release of their constituting ions. To simulate such behavior, our samples were incubated in PBS at 37 °C for 56 days (see section 2.6 for the experimental details). The bone healing process is a complex phenomenon which can take from a few weeks to some months, depending on the characteristics of both the patients and the defects [57]; nevertheless, 8 weeks is typically considered as a representative time for a bone fracture to heal, thus it was selected as the end point of our experiment. After the experiment, all samples preserved their macroscopic shape and could be easily recovered from the medium (see Figure S6). The morphology of the samples after the dissolution test was examined, and the micrographs are given in Figure S7. Interestingly, all samples display interconnected struvite crystals, confirming that the cement binding phase is still present after soaking in PBS. MPC_$SrCl_2$ (Figure S7C) does not show anymore its peculiar structure observed in Figure 3D and E: we can hypothesize that the structure observed in the sample before incubation favors the dissolution of the cement matrix and $SrCl_2$, resulting in the higher dissolution degree of such sample.

The extent of the dissolution was estimated by calculating the weight loss % of the samples after incubation. The results reported in Table S2 show that MPC_0.5 displays a limited weight loss (~3%), in line with the expected value for TMP_0, as we reported in previous investigations on similar samples [58,59]. Samples MPC_1 and MPC_$SrHPO_4$ show a slightly higher weight loss (~8% and 9%, respectively). Out of note, MPC_$SrCl_2$ loses about 1/3 of its initial weight, and this might be attributed to the high solubility of $SrCl_2 \cdot 6H_2O$ in water (54.7 g/100 mL at 25 °C) [60].

The amount of Mg^{2+} and Sr^{2+} released in time was analyzed by ICP-AES, and the cumulative concentrations of the two ions in PBS are reported in Figure 4. As a general comment, the amount of Mg^{2+} and Sr^{2+} released from the cements is limited, and this is consistent with the fact that the MPCs do not massively dissolve when incubated in water but are able to maintain their shape and integrity. MPC_0.5 and MPC_1 samples display a similar curve, suggesting that their dissolution behavior is alike. For MPC_$SrHPO_4$, the initial release of Mg^{2+} is more abrupt, and this is even more evident in MPC_$SrCl_2$: in this case, both Mg^{2+} and Sr^{2+} are immediately released from the cement matrix, and their concentration in PBS is more than twice than the other Sr-MPCs. This result is in agreement with the higher weight loss observed for this sample at the end of the experiment, as we pointed out at the beginning of this section. We already hypothesized that this peculiar behavior might be due to the fast dissolution of $SrCl_2 \cdot 6H_2O$, but the fact that the released Mg^{2+} is also significantly higher than the other samples suggests that the whole cement matrix is more prone to dissolution. Figure S8 shows the same data in which the amount of released Mg or Sr was normalized for the quantity initially present in the cements. The % of released ions after 56 days of incubation is below 7% for Mg and 4% for Sr, confirming that the majority of ions is retained in the cement matrix as a structural component. It is worth mentioning that, when applied *in vivo*, it is expected that the solubility-driven (passive) dissolution would be accompanied by the (active) action of bone cells that would contribute to resorb the materials while simultaneously producing new bone [61].

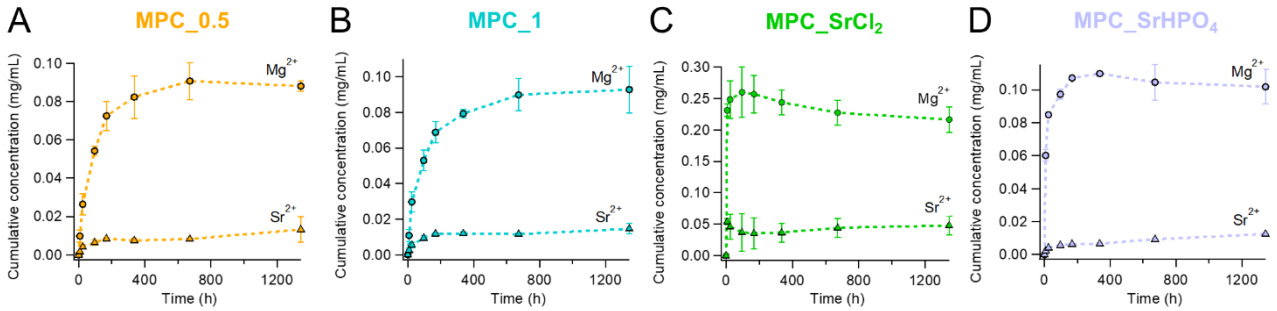

Figure 4. Cumulative concentration of Mg^{2+} (dots) and Sr^{2+} (triangles) in PBS vs time for MPC_0.5 (A), MPC_1 (B), MPC_$SrCl_2$ (C) and MPC_$SrHPO_4$ (D). The results are reported as average ± SD of three independent experiments. The points where the error bars are not visible have a SD smaller than the markers.

3.4 Injectability, anti-washout tests and inclusion of polymeric additives

The possibility of molding and injecting MPCs is one of their most attractive features, allowing for their application in mini-invasive surgery. This aspect is though critical in phosphate-based bone cements, and

difficulties in injection and phase separation phenomena are often reported [31,32]. Ideally, a bone cement should be easily injected by hand, and the extruded paste should maintain the desired shape and the features of the material loaded in the syringe; moreover, these characteristics should be preserved even when injecting the paste in aqueous media, since bone tissue is highly vascularized [62].

A preliminary idea of the behavior of our MPCs upon injection was obtained by manually extruding them from a syringe on graph paper after 5 min of setting and observing the outcome. The photos in Figure 5A show that samples MPC_0 and MPC_$SrCl_2$ can be extruded only to a limited extent, while for MPC_0.5 and MPC_$SrHPO_4$ the amount of extruded paste is higher. Sample MPC_1 shows phase separation, as only a small amount of liquid-like component of the paste is extruded from the syringe. In all cases, not all the paste loaded in the syringe can be extruded, as we observe a progressive hardening of the cement while pressing the plunger.

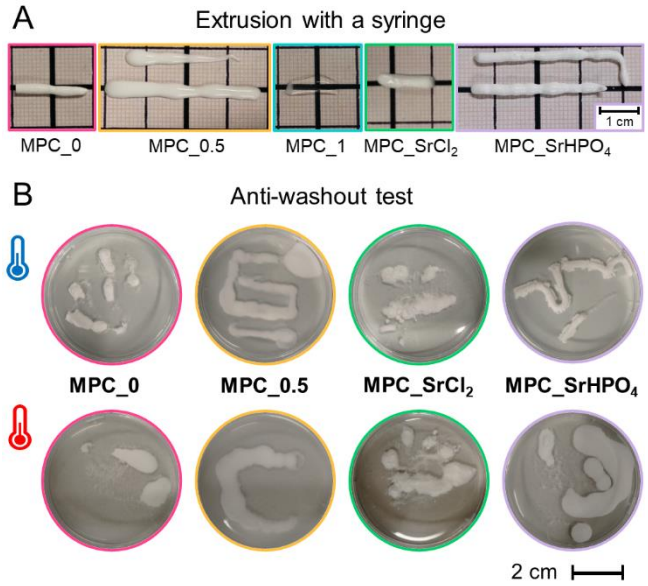

Figure 5. A) Photos of the MPCs extruded from a syringe after 5 min from the mixing. B) Photos of the MPCs extruded in a Petri dish with Ringer solution at RT (top) and 37 °C (bottom). This test was not carried out for sample MPC_1, due to the massive phase separation that occurs upon extrusion.

An idea of the quality of the extruded paste can be obtained by measuring the diameter of the material after the extrusion from the syringe: since the aperture size is 2 mm, the more the spreading diameter of the extruded material differs from that value, the more spreading of the paste will occur, meaning that the extruded paste is not able to preserve its shape. The results given in Figure 6A (grey bars) show that MPC_0.5 and MPC_1 display a significant spreading degree, while MPC_0, MPC_$SrCl_2$ and MPC_$SrHPO_4$ are more prone to preserve their shape.

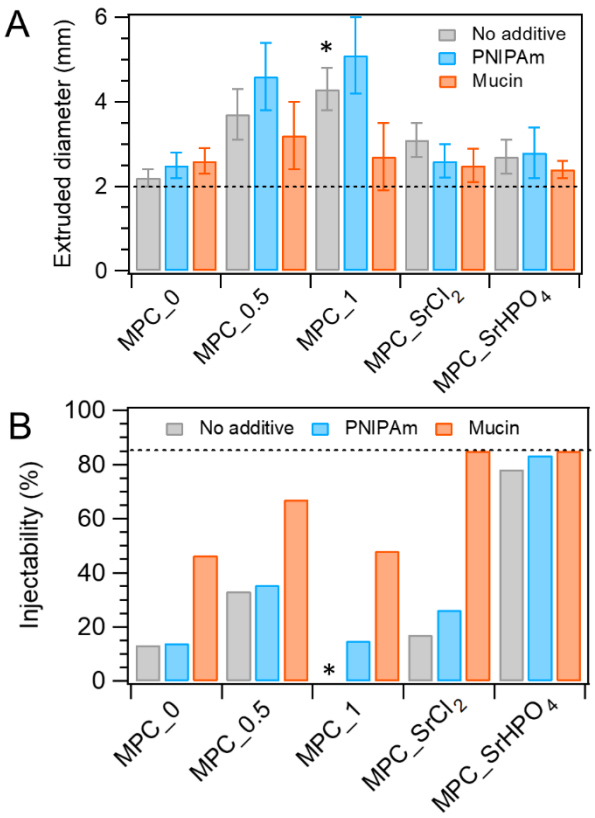

Figure 6. A) Diameter of the extruded pastes shown in Figure 5A (no additive) and 7A (PNIPAm and mucin), measured with ImageJ. Grey: no additive, blue: PNIPAm, orange: mucin. Each value is the average ± SD of 20 measurements along the extruded material. The dashed line at 2 mm indicates the aperture size of the syringe, *i.e.*, the ideal value to achieve. The sample indicated with * undergoes massive phase separation upon extrusion. B) Injectability % values calculated according to Equation 1. The dashed line at I(%)=85% indicates the maximum injectability value that can be reached with our setup. Sample MPC_1 without additive undergoes phase separation.

The amount of extruded paste was determined by means of injectability tests (see section 2.5.8), and the results are reported in Figure 6B (grey bars). In agreement with the qualitative observations previously discussed, MPC_0 and MPC_$SrCl_2$ show low injectability values (13% and 17%, respectively). The result obtained for MPC_1 (6%) is not meaningful as phase separation occurs in this case. Sample MPC_$SrHPO_4$ displays a remarkable injectability (78%). We recall that in our system, taking into account the dead volume of the syringe, a I(%) of 85% should be considered the maximum value attainable (see the details in section 2.5.8). We also evaluated the behavior of our MPCs by extruding the pastes directly in Ringer solution, both at RT and 37 °C (anti-washout tests). The photos of the systems taken after 30 min from the extrusion are reported in Figure 5B: for all samples, the outcome of the test was not satisfying, as all samples display a high level of spreading and dissolution in the medium. Only MPC_$SrHPO_4$ at RT can partially retain its shape after extrusion.

Since the injectability performances of our Sr-MPCs were not satisfying for a clinical application as bone cements, we tried to improve such aspect by introducing polymeric additives to the formulations. PNIPAm

and mucin were chosen to this purpose for the reasons highlighted in the Introduction. We evaluated the setting time of the MPCs prepared with the additives and the results reported in Table S3 show that when including polymers in the formulations, no dramatic modification in the setting times occurs, except for MPC_0.5, in which both t_1 and t_2 are significantly delayed upon the inclusion of both PNIPAm and mucin. The chemical and morphological properties of the set cements were evaluated by FTIR (Figure S9) and FE-SEM (Figure S10). FTIR spectra show no modifications in MPCs' characteristic peaks, suggesting that the inclusion of the polymers does not affect the phase composition of the cements. Moreover, the signals of the polymers are not visible in the spectra of the MPCs, probably due to the low amount and peaks superimpositions. Concerning the morphology, FE-SEM micrographs given in Figure S10 display very heterogenous structures, similar to those shown in Figure 3. The polymers can be detected in some regions of the MPC but, as a general comment, they appear well distributed within the inorganic phase.

The effect of the polymeric additives on the consistency and injectability of the pastes was determined by observing the appearance of the extruded materials. Both additives remarkably improve the quality and quantity of the extruded MPCs, as it can be observed from the photos in Figure 7A. Out of note, both PNIPAm and mucin make it possible to extrude MPC_1, which resulted in severe phase separation in the absence of additives (see Figure 5A). The spreading degree was evaluated, and the data shown in Figure 6A indicate different behaviors according to the polymers used: the inclusion of PNIPAm slightly increases the spreading of the extruded paste for all samples but MPC_$SrCl_2$. Mucin, on the other hand, lowers the extruded diameter for all samples but MPC_0, being thus more effective in improving the quality of the extruded material. The injectability tests showed a great improvement of I(%), in particular when using mucin: the results of the test given in Figure 6B show that PNIPAm (blue bars) mildly improves the injectability for MPC_1, MPC_$SrCl_2$ and MPC_$SrHPO_4$, while leaving unaltered MPC_0 and MPC_0.5. Mucin (orange bars) is way more effective in increasing the amount of extruded paste for all samples, and for MPC_$SrCl_2$ and MPC_$SrHPO_4$ it allows to achieve a I(%) of 85% that, considering the dead volume of the syringe, means a complete extrusion. The anti-washout tests were also carried out, to understand if polymer inclusion would improve the quality of the extruded material when in contact with aqueous media. The results shown in Figure 7B must be compared with those obtained for the MPCs without additives given in Figure 5B (top row, RT experiments). We observe a general improvement of the quality of the extruded material, especially when using mucin. At 37 °C, the results are similar to RT experiments (see Figure S11, in which the results of the anti-washout tests for all samples are compared). It has to be pointed out that even if the shape of the extruded material is not perfectly retained in the Ringer solution, in a potential application as bone cement the paste would be extruded in a more confined environment which, despite being highly vascularized, would not be as challenging as the conditions of this test.

In summary, the inclusion of polymeric additives is an effective strategy to improve the injectability and the extrusion quality of all Sr-MPCs. Among the two polymers tested, mucin is the most promising one. The inclusion of PNIPAm did not have the aspired outcome, as only minor improvements in injectability were detected and the results of the anti-washout experiments at 37 °C were not satisfying: we hypothesize that

when mixed with the MPCs components, PNIPAm is not able to self-assemble to result in a gel-like material, not being able to tighten and confine the cementitious matrix.

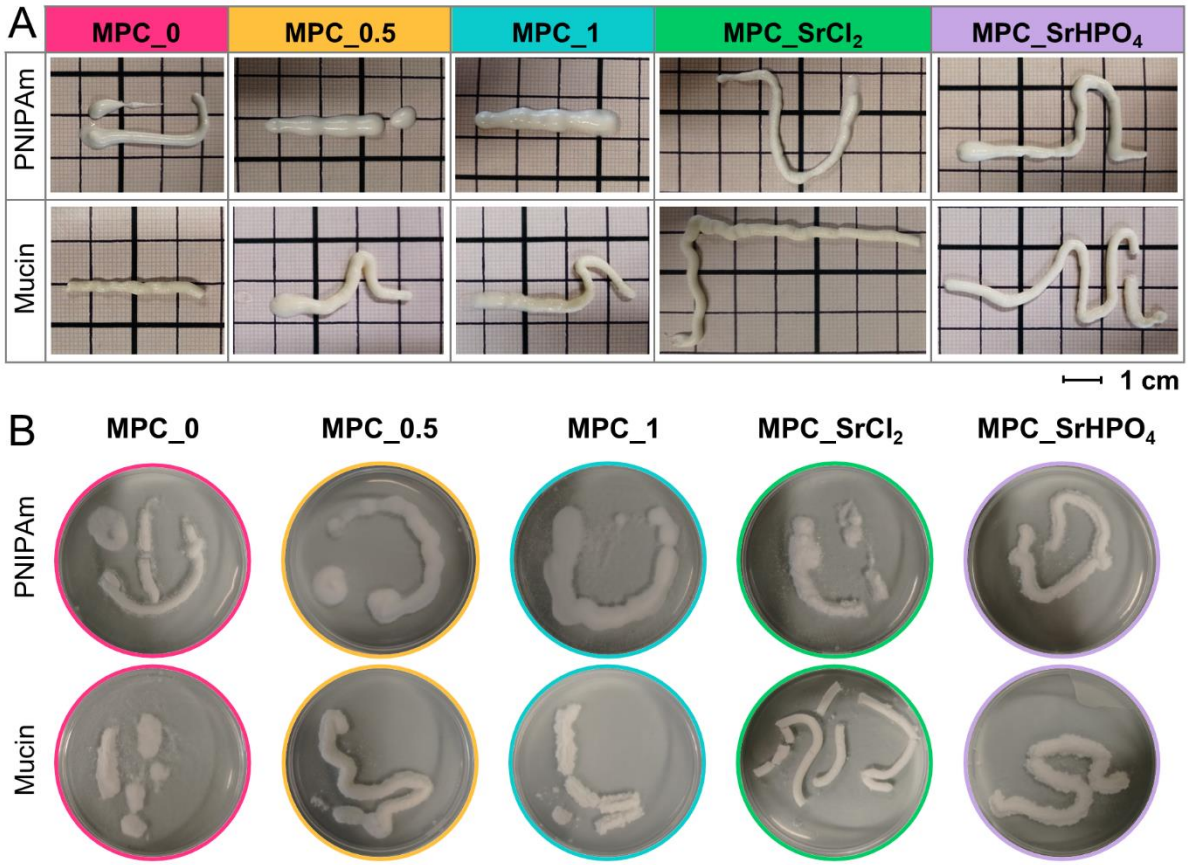

Figure 7. A) Photos of the Sr-MPCs prepared with 10 % w/v of PNIPAm (top row) and mucin (bottom row) extruded from a syringe after 5 min of setting. B) Results of the anti-washout test at room temperature performed by extruding the cements after 5 min from the mixing directly in the Ringer solution.

4. Conclusions

This work describes the preparation and characterization of MPCs including Sr ions and polymeric additives, designed for applications as bone cements. Sr was incorporated in the formulations in different forms, namely using a Sr-substituted TMP powder as a precursor or adding $SrCl_2$ and $SrHPO_4$ to the cement paste. The different Sr-MPCs were characterized and compared with a control sample consisting of a Sr-free MPC. The properties of the pastes (cohesion and setting time) are dependent on the type of sample, suggesting a strategy to control them using a different Sr precursor. The results also showed that in all samples the binding phase consists of struvite ($MgNH_4PO_4 \cdot 6H_2O$), even if the formed amount changes according to the Sr precursor, as revealed by thermal analysis. An incubation test in PBS at physiological temperature gave information on the dissolution and release kinetics of the different Sr-MPCs. Out of note, the amount and kinetics of the released Sr and Mg can be tuned according to the formulation. In particular, the use of $SrCl_2$ in the formulation leads to a higher dissolution and a fast release of a significant amount of both Sr and Mg, compared to the other samples. Concerning the injectability of the cement pastes, which is a fundamental parameter to use MPCs as

fillers for bone defects, all samples but MPC_$SrHPO_4$ showed unsatisfactory performances, in particular an injectability % below 30% and a significant increase in the spreading diameter of the paste upon extrusion. To tackle this issue, we included two different polymeric additives (PNIPAm and mucin) in the cement formulation, leading to a remarkable increase in the injectability % value, especially when using mucin. This polymer, which is known for its lubricating properties, facilitates the extrusion process and allows to reach a complete injectability for MPC_$SrCl_2$ and MPC_$SrHPO_4$, while it also allows for the extrusion of a significant amount of sample MPC_1, that undergoes massive phase separation when no polymeric additive is present. The presence of the polymeric additives in the formulations also improves the anti-washout properties of the cements, namely the cohesion extent when injected in an aqueous medium.

To sum up, the present study showcases the possibility of preparing Sr-containing MPCs endowed with different properties according to the Sr precursor used in the formulation. The presence of Sr, which is known to promote bone regeneration and whose release can be tuned according to its inclusion form in MPC, makes such systems attractive for use as bone cements; moreover, we also demonstrated that the addition of mucin to such formulations contributes to improve the characteristics of the pastes, overcoming one of the main limitations of such materials and paving the way for their use in clinics. As a future perspective, the study of the dissolution kinetics of the different MPCs, both pristine and including polymeric additives, could be of interest, as well as the assessment of the effect of mucin on both the dissolution and release profile of the cements.

Acknowledgements

CSGI consortium, MUR PRIN - 2017249YEF and MIUR-Italy ("Progetto Dipartimenti di Eccellenza 2018-2022" allocated to Department of Chemistry "Ugo Schiff") are acknowledged for financial support. Prof. Mirko Severi from the University of Florence is acknowledged for ICP-AES measurements.

References

[1] J. Jeong, J.H. Kim, J.H. Shim, N.S. Hwang, C.Y. Heo, Bioactive calcium phosphate materials and applications in bone regeneration, Biomater Res. 23 (2019). https://doi.org/10.1186/s40824-018-0149-3.

[2] N. Ostrowski, A. Roy, P.N. Kumta, Magnesium Phosphate Cement Systems for Hard Tissue Applications: A Review, ACS Biomater. Sci. Eng. 2 (2016) 1067–1083. https://doi.org/10.1021/acsbiomaterials.6b00056.

[3] X. Gu, Y. Li, C. Qi, K. Cai, Biodegradable magnesium phosphates in biomedical applications, J. Mater. Chem. B. 10 (2022) 2097–2112. https://doi.org/10.1039/D1TB02836G.

[4] K. Bavya Devi, V. Lalzawmliana, M. Saidivya, V. Kumar, M. Roy, S. Kumar Nandi, Magnesium Phosphate Bioceramics for Bone Tissue Engineering, The Chemical Record. n/a (n.d.) e202200136. https://doi.org/10.1002/tcr.202200136.

[5] H. Zhou, B. Liang, H. Jiang, Z. Deng, K. Yu, Magnesium-based biomaterials as emerging agents for bone repair and regeneration: from mechanism to application, Journal of Magnesium and Alloys. 9 (2021) 779–804. https://doi.org/10.1016/j.jma.2021.03.004.

[6] M. Nabiyouni, T. Brückner, H. Zhou, U. Gbureck, S.B. Bhaduri, Magnesium-based bioceramics in orthopedic applications, Acta Biomaterialia. 66 (2018) 23–43. https://doi.org/10.1016/j.actbio.2017.11.033.

[7] S. Meininger, C. Moseke, K. Spatz, E. März, C. Blum, A. Ewald, E. Vorndran, Effect of strontium substitution on the material properties and osteogenic potential of 3D powder printed magnesium phosphate scaffolds, Materials Science and Engineering: C. 98 (2019) 1145–1158. https://doi.org/10.1016/j.msec.2019.01.053.

[8] N.J. Lakhkar, I.-H. Lee, H.-W. Kim, V. Salih, I.B. Wall, J.C. Knowles, Bone formation controlled by biologically relevant inorganic ions: Role and controlled delivery from phosphate-based glasses, Advanced Drug Delivery Reviews. 65 (2013) 405–420. https://doi.org/10.1016/j.addr.2012.05.015.

[9] Y. Deng, W. Wei, P. Tang, Applications of Calcium-Based Nanomaterials in Osteoporosis Treatment, ACS Biomater. Sci. Eng. 8 (2022) 424–443. https://doi.org/10.1021/acsbiomaterials.1c01306.

[10] D. Marx, A. Rahimnejad Yazdi, M. Papini, M. Towler, A review of the latest insights into the mechanism of action of strontium in bone, Bone Reports. 12 (2020) 100273. https://doi.org/10.1016/j.bonr.2020.100273.

[11] X. Liu, H. Huang, J. Zhang, T. Sun, W. Zhang, Z. Li, Recent Advance of Strontium Functionalized in Biomaterials for Bone Regeneration, Bioengineering. 10 (2023) 414. https://doi.org/10.3390/bioengineering10040414.

[12] G. Borciani, G. Ciapetti, C. Vitale-Brovarone, N. Baldini, Strontium Functionalization of Biomaterials for Bone Tissue Engineering Purposes: A Biological Point of View, Materials. 15 (2022) 1724. https://doi.org/10.3390/ma15051724.

[13] M.H. Alkhraisat, C. Rueda, J. Cabrejos-Azama, J. Lucas-Aparicio, F.T. Mariño, J. Torres García-Denche, L.B. Jerez, U. Gbureck, E.L. Cabarcos, Loading and release of doxycycline hyclate from strontium-substituted calcium phosphate cement, Acta Biomaterialia. 6 (2010) 1522–1528. https://doi.org/10.1016/j.actbio.2009.10.043.

[14] A. Lode, C. Heiss, G. Knapp, J. Thomas, B. Nies, M. Gelinsky, M. Schumacher, Strontium-modified premixed calcium phosphate cements for the therapy of osteoporotic bone defects, Acta Biomaterialia. 65 (2018) 475–485. https://doi.org/10.1016/j.actbio.2017.10.036.

[15] M. Schumacher, M. Gelinsky, Strontium modified calcium phosphate cements – approaches towards targeted stimulation of bone turnover, J. Mater. Chem. B. 3 (2015) 4626–4640. https://doi.org/10.1039/C5TB00654F.

[16] M. Schumacher, A. Henß, M. Rohnke, M. Gelinsky, A novel and easy-to-prepare strontium(II) modified calcium phosphate bone cement with enhanced mechanical properties, Acta Biomaterialia. 9 (2013) 7536–7544. https://doi.org/10.1016/j.actbio.2013.03.014.

[17] S. Panzavolta, P. Torricelli, L. Sturba, B. Bracci, R. Giardino, A. Bigi, Setting properties and in vitro bioactivity of strontium-enriched gelatin–calcium phosphate bone cements, J. Biomed. Mater. Res. 84A (2008) 965–972. https://doi.org/10.1002/jbm.a.31412.

[18] H. Xu, L. Zhu, F. Tian, C. Wang, W. Wu, B. Lu, L. Yan, S. Jia, D. Hao, In Vitro and In Vivo Evaluation of Injectable Strontium-Modified Calcium Phosphate Cement for Bone Defect Repair in Rats, International Journal of Molecular Sciences. 24 (2023) 568. https://doi.org/10.3390/ijms24010568.

[19] G.-M. Kuang, W. p. Yau, W.M. Lam, J. Wu, K.Y. Chiu, W.W. Lu, H. Pan, An effective approach by a chelate reaction in optimizing the setting process of strontium-incorporated calcium phosphate bone cement, Journal of Biomedical Materials Research Part B: Applied Biomaterials. 100B (2012) 778–787. https://doi.org/10.1002/jbm.b.32511.

[20] G.-M. Kuang, W.P. Yau, J. Wu, K.W.K. Yeung, H. Pan, W.M. Lam, W.W. Lu, K.Y. Chiu, Strontium exerts dual effects on calcium phosphate cement: Accelerating the degradation and enhancing the osteoconductivity both in vitro and in vivo, Journal of Biomedical Materials Research Part A. 103 (2015) 1613–1621. https://doi.org/10.1002/jbm.a.35298.

[21] M. Dapporto, D. Gardini, A. Tampieri, S. Sprio, Nanostructured Strontium-Doped Calcium Phosphate Cements: A Multifactorial Design, Applied Sciences. 11 (2021) 2075. https://doi.org/10.3390/app11052075.

[22] M. Dapporto, M. Tavoni, E. Restivo, F. Carella, G. Bruni, L. Mercatali, L. Visai, A. Tampieri, M. Iafisco, S. Sprio, Strontium-doped apatitic bone cements with tunable antibacterial and antibiofilm ability, Frontiers in Bioengineering and Biotechnology. 10 (2022). https://www.frontiersin.org/articles/10.3389/fbioe.2022.969641.

[23] K. Sarkar, V. Kumar, K.B. Devi, D. Ghosh, S.K. Nandi, M. Roy, Effects of Sr doping on biodegradation and bone regeneration of magnesium phosphate bioceramics, Materialia. 5 (2019) 100211. https://doi.org/10.1016/j.mtla.2019.100211.

[24] F. He, T. Lu, X. Fang, C. Qiu, Y. Tian, Y. Li, F. Zuo, J. Ye, Study on MgxSr3-x(PO4)2 bioceramics as potential bone grafts, Colloids and Surfaces B: Biointerfaces. 175 (2019) 158–165. https://doi.org/10.1016/j.colsurfb.2018.11.085.

[25] F. He, T. Lu, X. Fang, Y. Li, F. Zuo, X. Deng, J. Ye, Effects of strontium amount on the mechanical strength and cell-biological performance of magnesium-strontium phosphate bioceramics for bone regeneration, Materials Science and Engineering: C. 112 (2020) 110892. https://doi.org/10.1016/j.msec.2020.110892.

[26] C. Moseke, K. Wimmer, M. Meininger, J. Zerweck, C. Wolf-Brandstetter, U. Gbureck, A. Ewald, Osteoclast and osteoblast response to strontium-doped struvite coatings on titanium for improved bone integration, Biomedical Engineering / Biomedizinische Technik. 65 (2020) 631–641. https://doi.org/10.1515/bmt-2019-0265.

[27] M. Meininger, C. Wolf-Brandstetter, J. Zerweck, F. Wenninger, U. Gbureck, J. Groll, C. Moseke, Electrochemically assisted deposition of strontium modified magnesium phosphate on titanium surfaces, Materials Science and Engineering: C. 67 (2016) 65–71. https://doi.org/10.1016/j.msec.2016.04.102.

[28] X. Fang, Z. Shi, F. He, C. Qiu, Y. Tian, J. Ye, Fabrication of interconnected strontium-containing magnesium phosphate bioceramic scaffolds based on free microspheres accumulation, Ceramics International. 45 (2019) 22409–22412. https://doi.org/10.1016/j.ceramint.2019.07.192.

[29] S. Dutta, R. Khan, N.S. Prakash, S. Gupta, D. Ghosh, S.K. Nandi, M. Roy, In Vitro Degradation and In Vivo Biocompatibility of Strontium-Doped Magnesium Phosphate-Reinforced Magnesium Composites, ACS Biomater. Sci. Eng. 8 (2022) 4236–4248. https://doi.org/10.1021/acsbiomaterials.2c00142.

[30] S. Meininger, S. Mandal, A. Kumar, J. Groll, B. Basu, U. Gbureck, Strength reliability and in vitro degradation of three-dimensional powder printed strontium-substituted magnesium phosphate scaffolds, Acta Biomaterialia. 31 (2016) 401–411. https://doi.org/10.1016/j.actbio.2015.11.050.

[31] R. O'Neill, H.O. McCarthy, E. Cunningham, E. Montufar, M.-P. Ginebra, D.I. Wilson, A. Lennon, N. Dunne, Extent and mechanism of phase separation during the extrusion of calcium phosphate pastes, J Mater Sci: Mater Med. 27 (2016) 29. https://doi.org/10.1007/s10856-015-5615-z.

[32] R. O'Neill, H.O. McCarthy, E.B. Montufar, M.-P. Ginebra, D.I. Wilson, A. Lennon, N. Dunne, Critical review: Injectability of calcium phosphate pastes and cements, Acta Biomaterialia. 50 (2017) 1–19. https://doi.org/10.1016/j.actbio.2016.11.019.

[33] A.-M. Yousefi, A review of calcium phosphate cements and acrylic bone cements as injectable materials for bone repair and implant fixation, Journal of Applied Biomaterials & Functional Materials. 17 (2019) 228080001987259. https://doi.org/10.1177/2280800019872594.

[34] S. Tadier, L. Galea, B. Charbonnier, G. Baroud, M. Bohner, Phase and size separations occurring during the injection of model pastes composed of β-tricalcium phosphate powder, glass beads and aqueous solutions, Acta Biomaterialia. 10 (2014) 2259–2268. https://doi.org/10.1016/j.actbio.2013.12.018.

[35] M.P. Ginebra, A. Rilliard, E. Fernández, C. Elvira, J. San Román, J.A. Planell, Mechanical and rheological improvement of a calcium phosphate cement by the addition of a polymeric drug, J Biomed Mater Res. 57 (2001) 113–118. https://doi.org/10.1002/1097-4636(200110)57:1<113::aid-jbm1149>3.0.co;2-5.

[36] M. Bohner, G. Baroud, Injectability of calcium phosphate pastes, Biomaterials. 26 (2005) 1553–1563. https://doi.org/10.1016/j.biomaterials.2004.05.010.

[37] L. Chen, H. Xiang, X.X. Li, J.D. Ye, X.P. Wang, L. Li, X.M. Zhang, Development of a New Injectable Calcium Phosphate Cement That Contains Modified Starch, Key Engineering Materials. 330–332 (2007) 843–846. https://doi.org/10.4028/www.scientific.net/KEM.330-332.843.

[38] H.-J. Lee, B. Kim, A.R. Padalhin, B.-T. Lee, Incorporation of chitosan-alginate complex into injectable calcium phosphate cement system as a bone graft material, Materials Science and Engineering: C. 94 (2019) 385–392. https://doi.org/10.1016/j.msec.2018.09.039.

[39] Y. Xie, J. Liu, S. Cai, X. Bao, Q. Li, G. Xu, Setting Characteristics and High Compressive Strength of an Anti-washout, Injectable Calcium Phosphate Cement Combined with Thermosensitive Hydrogel, Materials. 13 (2020) 5779. https://doi.org/10.3390/ma13245779.

[40] N. Ribeiro, M. Reis, L. Figueiredo, A. Pimenta, L.F. Santos, A.C. Branco, A.P. Alves de Matos, M. Salema-Oom, A. Almeida, M.F.C. Pereira, R. Colaço, A.P. Serro, Improvement of a commercial calcium phosphate bone cement by means of drug delivery and increased injectability, Ceramics International. 48 (2022) 33361–33372. https://doi.org/10.1016/j.ceramint.2022.07.279.

[41] L. Yu, K. Xia, C. Gong, J. Chen, W. Li, Y. Zhao, W. Guo, H. Dai, An injectable bioactive magnesium phosphate cement incorporating carboxymethyl chitosan for bone regeneration, International Journal of Biological Macromolecules. 160 (2020) 101–111. https://doi.org/10.1016/j.ijbiomac.2020.05.161.

[42] F. Doberenz, K. Zeng, C. Willems, K. Zhang, T. Groth, Thermoresponsive polymers and their biomedical application in tissue engineering – a review, Journal of Materials Chemistry B. 8 (2020) 607–628. https://doi.org/10.1039/C9TB02052G.

[43] C.E. Wagner, K.M. Wheeler, K. Ribbeck, Mucins and Their Role in Shaping the Functions of Mucus Barriers, Annu. Rev. Cell Dev. Biol. 34 (2018) 189–215. https://doi.org/10.1146/annurev-cellbio-100617-062818.

[44] C. Moseke, V. Saratsis, U. Gbureck, Injectability and mechanical properties of magnesium phosphate cements, J Mater Sci Mater Med. 22 (2011) 2591–2598. https://doi.org/10.1007/s10856-011-4442-0.

[45] X. Yang, X. Li, J. Dong, Farringtonite as an efficient catalyst for linear-chain α-olefin epoxidation with aqueous hydrogen peroxide, New Journal of Chemistry. 45 (2021) 11968–11976. https://doi.org/10.1039/D1NJ01872H.

[46] D. Bingöl, S. Aydoğan, S.K. Bozbaş, Production of SrCO3 and (NH4)2SO4 by the dry mechanochemical processing of celestite, Journal of Industrial and Engineering Chemistry. 18 (2012) 834–838. https://doi.org/10.1016/j.jiec.2011.11.145.

[47] K. Zheng, T. Chen, J. Zhang, X. Tian, H. Ge, T. Qiao, J. Lei, X. Li, T. Duan, W. Zhu, Nano-Montmorillonite Regulated Crystallization of Hierarchical Strontium Carbonate in a Microbial Mineralization System, Materials. 12 (2019) 1392. https://doi.org/10.3390/ma12091392.

[48] I. Arvanitidis, D. Sichen, S. Seetharaman, H.Y. Sohn, The intrinsic thermal decomposition kinetics of SrCO3 by a nonisothermal technique, Metall Mater Trans B. 28 (1997) 1063–1068. https://doi.org/10.1007/s11663-997-0060-0.

[49] J.S. Kruger, R.J. Dreiling, D.G. Wilcox, A.J. Ringsby, K.L. Noon, C.K. Amador, D.G. Brandner, K.J. Ramirez, S.J. Haugen, B.C. Klein, R. Davis, R.J. Hanes, R.M. Happs, N.S. Cleveland, E.D. Christensen, J. Miscall, G.T. Beckham, Lignin alkaline oxidation using reversibly-soluble bases, Green Chem. 24 (2022) 8733–8741. https://doi.org/10.1039/D2GC03333J.

[50] S.V. Dorozhkin, Self-Setting Calcium Orthophosphate Formulations: Cements, Concretes, Pastes and Putties, International Journal of Materials and Chemistry. 1 (2012) 1–48. https://doi.org/10.5923/j.ijmc.20110101.01.

[51] R. Gelli, L. Mati, F. Ridi, P. Baglioni, Tuning the properties of magnesium phosphate-based bone cements: Effect of powder to liquid ratio and aqueous solution concentration, Materials Science and Engineering: C. 95 (2019) 248–255. https://doi.org/10.1016/j.msec.2018.10.083.

[52] R. Gelli, M. Tonelli, F. Martini, L. Calucci, S. Borsacchi, F. Ridi, Effect of borax on the hydration and setting of magnesium phosphate cements, Construction and Building Materials. 348 (2022) 128686. https://doi.org/10.1016/j.conbuildmat.2022.128686.

[53] W. Han, Y. Zhang, R. Liu, Y. Sun, M. Li, Purification of spent electrolyte by sequential precipitation method and its on-line monitoring, Ionics. 27 (2021) 4829–4838. https://doi.org/10.1007/s11581-021-04256-x.

[54] D. Sidorczuk, M. Kozanecki, B. Civalleri, K. Pernal, J. Prywer, Structural and Optical Properties of Struvite. Elucidating Structure of Infrared Spectrum in High Frequency Range, J Phys Chem A. 124 (2020) 8668–8678. https://doi.org/10.1021/acs.jpca.0c04707.

[55] M.V. Ramlogan, A.A. Rouff, An investigation of the thermal behavior of magnesium ammonium phosphate hexahydrate, J Therm Anal Calorim. 123 (2016) 145–152. https://doi.org/10.1007/s10973-015-4860-1.

[56] J. Hövelmann, T.M. Stawski, R. Besselink, H.M. Freeman, K.M. Dietmann, S. Mayanna, B.R. Pauw, L.G. Benning, A template-free and low temperature method for the synthesis of mesoporous magnesium phosphate with uniform pore structure and high surface area, Nanoscale. 11 (2019) 6939–6951. https://doi.org/10.1039/C8NR09205B.

[57] L. Claes, S. Recknagel, A. Ignatius, Fracture healing under healthy and inflammatory conditions, Nat Rev Rheumatol. 8 (2012) 133–143. https://doi.org/10.1038/nrrheum.2012.1.

[58] R. Gelli, G. Di Pompo, G. Graziani, S. Avnet, N. Baldini, P. Baglioni, F. Ridi, Unravelling the Effect of Citrate on the Features and Biocompatibility of Magnesium Phosphate-Based Bone Cements, ACS Biomater. Sci. Eng. 6 (2020) 5538–5548. https://doi.org/10.1021/acsbiomaterials.0c00983.

[59] M. Tonelli, R. Gelli, F. Ridi, P. Baglioni, Magnesium phosphate-based cements containing Halloysite nanotubes for cracks repair, Construction and Building Materials. 301 (2021) 124056. https://doi.org/10.1016/j.conbuildmat.2021.124056.

[60] W.M. Haynes, D.R. Lide, T.J. Bruno, CRC handbook of chemistry and physics: a ready reference book of chemical and physical data, 93rd ed, CRC, Boca Raton, 2012.

[61] B. Kanter, M. Geffers, A. Ignatius, U. Gbureck, Control of in vivo mineral bone cement degradation, Acta Biomaterialia. 10 (2014) 3279–3287. https://doi.org/10.1016/j.actbio.2014.04.020.

[62] C. Carulli, M. Innocenti, M.L. Brandi, Bone Vascularization in Normal and Disease Conditions, Frontiers in Endocrinology. 4 (2013). https://www.frontiersin.org/articles/10.3389/fendo.2013.00106.